J Solid State Electrochem (2011) 15:1287–1294
DOI 10.1007/s10008-010-1218-2

ORIGINAL PAPER

Electrocatalytic interaction of nano-engineered palladium on carbon nanofibers with hydrogen peroxide and β-NADH

Zhan Lin · Liwen Ji · Andrew J. Medford · Quan Shi · Wendy E. Krause · Xiangwu Zhang

Received: 3 August 2010 / Revised: 3 October 2010 / Accepted: 10 October 2010 / Published online: 27 October 2010

Abstract The growing demands for reagentless hydrogen peroxide (H_2O_2) and β-nicotinamide adenine dinucleotide (β-NADH) sensors from food, pharmaceutical, chemical, and biochemical fields have stimulated extensive research interest on nano-engineered Pd. In this paper, Pd/carbon composite nanofibers were prepared by electrodepositing Pd onto electrospun carbon nanofibers to act as a catalyst toward the electrocatalytic redox reactions of H_2O_2 and β-NADH. The morphology of nano-engineered Pd was controlled by selectively adjusting the electrodeposition time and potential. Scanning electron microscopy and transmission electron microscopy results showed that nanocactus- and nanoflower-like Pd depositions were obtained on the surface of carbon nanofibers. Electrocatalytic analysis demonstrated a high electrocatalytic activity of the composite nanofibers for the redox of H_2O_2 and oxidation of β-NADH.

Keywords Electrodeposition · Pd · Carbon nanofibers · Hydrogen peroxide · β-NADH

Introduction

Palladium can be used as a heterogeneous catalyst for low temperature catalytic reduction of automobile emissions and for Suzuki, Heck, and Stille coupling reactions, and it is also a good material for hydrogen storage and gas sensing applications [1–5]. Compared with traditional spherical Pd nanoparticles, nano-engineered Pd, which is typically prepared by electrochemical deposition at room temperature without template or surfactant, has unique nanostructure and higher surface activity. For example, Meng et al. produced anisotropic Pd single-crystal nanothorns using potential square wave electrodeposition and found that such nano-engineered Pd exhibited better catalytic performance for the oxidation of formic acid than commercial spherical Pd nanoparticles [6]. Moreover, Pd, assembled with suitable catalyst support, has shown great promises in fuel cells, electrical appliances, and highly accurate chemical/biological sensing applications [7–10]. For instance, Hu et al. reported the preparation of carbon-supported Pd nanoparticles, which showed large active surface area and high electrochemical activity for the oxidation of alcohol [11].

Due to the high surface area and excellent electrical/mechanical properties, carbon nanotubes (CNTs) are good material candidate for supporting catalytic metals, but they are relatively expensive [12]. Several approaches including electrodeposition, wet-chemical reduction, electrophoretic deposition, and electroless deposition have been developed to synthesize metal nanoparticle/CNT composites, which can be applied in diverse areas ranging from fuel cells, supercapacitors, hydrogen storage, field emission devices, to chemical/biological sensors [13–18]. Electrospun carbon nanofibers (CNFs), which can be simply produced by electrospinning and carbonizing polyacrylonitrile (PAN), have high mechanical strength, high thermal conductivity, and good electric properties, and they are also suitable as catalyst supports [19]. Compared with CNTs, CNFs are inexpensive and can be easily fabricated into different forms, such as porous nonwoven mats, continues yarns, and organized arrays, for

Z. Lin · L. Ji · A. J. Medford · Q. Shi · W. E. Krause · X. Zhang (✉)
Fiber and Polymer Science Program,
Department of Textile Engineering, Chemistry and Science,
North Carolina State University,
Raleigh, NC 27695-8301, USA
e-mail: xiangwu_zhang@ncsu.edu

practical applications [20–22]. Therefore, replacing CNTs with CNFs to support metallic catalysts can significantly lower the cost without sacrificing the electrocatalytic activity. So far, several researchers have prepared CNF-supported Pd catalysts; however, the Pd particles developed in these groups are in the form of spheres [23–27]. Switching spherical Pd particles to nano-engineered structures could significantly increase the accessible surface area and improve the electrocatalytic activity of Pd/CNFs. Thus, the technological impact of developing novel nano-engineered Pd on CNFs would be important and needs further exploration.

In this paper, the preparation and structure control of nanocactus- and nanoflower-like Pd/CNFs using the combination of electrospinning, carbonization, and electrodeposition techniques are discussed. These nano-engineered Pd/CNF composites possess high electrochemically active surface area and good conductivity, and they also have excellent electrocatalytic activities toward the redox of hydrogen peroxide (H_2O_2) and oxidation of β-nicotinamide adenine dinucleotide (β-NADH).

Experimental

Chemicals and reagents

PAN, palladium(II) chloride ($PdCl_2$), *N*,*N*-dimethylformamide (DMF), sulfuric acid (H_2SO_4), H_2O_2, β-NADH, and phosphate-buffered saline (PBS) solution in water (pH= 7.2) were purchased from Sigma-Aldrich and were used without further purification. Deionized water was used throughout.

Synthesis of carbon nanofibers

A DMF solution of 8 wt.% PAN was prepared at 60 °C, with mechanical stirring for 3.0 h. The electrospinning was conducted using a Gamma ES40P-20W/DAM variable high-voltage power supply under a voltage of 15 kV. Under such a high voltage, a polymer stream was ejected through a syringe and accelerated toward the nanofiber collector, during which the solvent was rapidly evaporated. Aluminum foil was placed over the collector plate of the electrospinning apparatus to collect electrospun PAN fibers. These PAN nanofibers were then stabilized in an air atmosphere at 280 °C for 2.0 h with a heating rate of 5.0 °C min^{-1} and carbonized at 700 °C for 1.0 h in nitrogen atmosphere with a heating rate of 2.0 °C min^{-1}. The resultant CNFs formed free-standing nonwoven membranes and were directly used as the working electrode in the electrodeposition of nano-engineered Pd.

Electrodeposition of nano-engineered Pd

CNFs were first cycled in 1.0 M H_2SO_4 solution between −0.70 and +1.20 V for 100 cycles at 50.0 mV s^{-1} to oxidize the surface. The electrodeposition of nano-engineered Pd was carried out by applying potentials of −0.2, −0.1, 0.0, +0.1, and +0.2 V (vs. Ag/AgCl/4.0 M KCl), respectively, with different deposition durations on the oxidized CNFs in 5.0 mM $PdCl_2$+1.0 M H_2SO_4 solutions.

Characterization

X-ray diffraction (XRD) analysis was performed with a Philips XLF ATPS XRD 100 diffractometer using CuKα radiation. The operating voltage and current were 40.0 kV and 60.0 mA, respectively. A crystal-monochromated collection system was used to acquire the diffractogram at 0.05° intervals at a rate of 0.5 s/step. The structure of CNFs and Pd/CNFs, which were collected on 200 mesh carbon-coated Cu grids, was evaluated using a Hitachi HF-2000 transmission electron microscopy (TEM) at 200 kV. The morphology of CNFs and Pd/CNFs was also observed with a JEOL JSM-6360LV FESEM at 15 kV. Brunauer–Emmett–Teller (BET) nitrogen adsorption method was used to evaluate the surface area of Pd/CNFs. The samples were degassed under flowing UHP grade nitrogen for 2.0 h at a temperature of 100 °C. Nitrogen gas adsorption measurements were taken at 0.05, 0.10, 0.15, 0.20, and 0.25 of saturation pressure using a Micromeritics Gemini 2360 instrument capable of measuring surface area from 0.01 m^2 g^{-1}. The helium method was used to analyze the free space in the analysis tube, and five pressure points were used to calculate the BET surface area. Electrochemical measurements of Pd/CNFs were performed in a three-electrode cell at 25 °C on an electrochemical workstation (AQ4 Gamry Reference 600, USA). The cell consisted of a working electrode (Pd/CNFs), a Pt counter electrode, and a reference electrode (Ag/AgCl/4.0 M KCl). Nitrogen was used to bubble the solutions for 30 min prior to taking measurements and was then used continually as a purge gas to protect the experiment environment. The reproducibility of electrochemical results was ensured by conducting all measurements on at least three cells.

Results and discussion

SEM and TEM images of Pd/CNFs

Scanning electron microscopy (SEM) images of nano-engineered Pd/CNFs, in which Pd was electrodeposited at −0.2 V for 4.0 h, are shown in Fig. 1. It is seen from Fig. 1a that cactus-like Pd is formed on the surface of CNFs. The

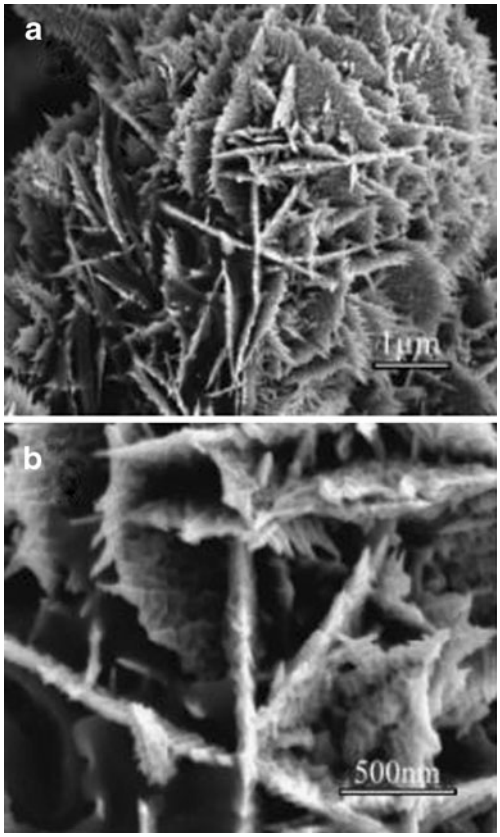

Fig. 1 SEM images of Pd/CNF nanocactus structure composed of nanotree-like clusters. Deposition potential, −0.2 V. Deposition time, 4.0 h

enlarged SEM image shown in Fig. 1b reveals that the three-dimensional cactus-like Pd structure is formed by numerous nanotree-like clusters within carbon nanofiber length.

Figure 2 shows TEM images of CNFs both before and after Pd deposition. Before electrodeposition, pure CNF is smooth and does not have surface particles. However, after 4.0 h of electrodeposition at −0.2 V, a nanotree-like Pd structure is formed, which agrees with the SEM results. The corresponding electron diffraction pattern shown in the inset of Fig. 2b and the energy dispersive X-ray spectroscopy (EDS) of Pd/CNFs in Fig. 2c confirm the presence of Pd on the CNF surface. The carbon peak in Fig. 2c comes from the CNF matrix, and the copper peak comes from the TEM sample grid used in the experiment.

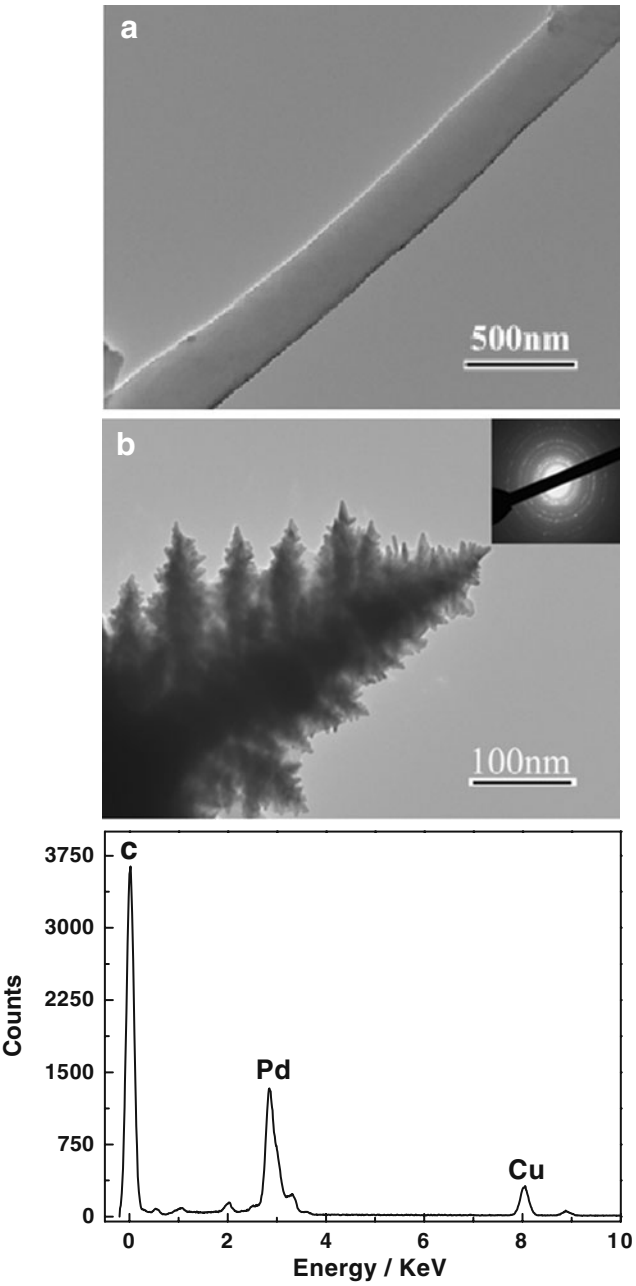

Fig. 2 TEM images of **a** CNF and **b** Pd/CNF and EDS spectrum of **c** Pd/CNF. The *inset* in **b** shows the electron diffraction pattern of the TEM image. Deposition potential, −0.2 V. Deposition time, 4.0 h

Electrodeposition growth and mechanism

To gain a complete view of Pd nanostructure formation mechanism, a morphological evolution study was conducted. Figure 3 shows TEM images of nano-engineered Pd/CNFs, in which Pd was deposited under −0.2 V with the duration of 1.0, 2.0, 4.0, and 8.0 h, respectively. As shown in Fig. 3a, after 1.0 h of deposition, nanosized snow-like Pd particles are formed on CNFs, which begin to aggregate when the deposition time increases to 2.0 h (Fig. 3b). After 4.0 h, Pd particles grow into tree-like structure, as shown in Fig. 3c. However, when the deposition time is 8.0 h, some branches in the nanotree-like structure start to merge due to the excessive deposition of Pd.

Based on the TEM results, Fig. 4 illustrates the evolution mechanism of Pd nanostructure on a CNF. In the initial stage, Pd nanonuclei are formed on the CNF surface through the electroreduction process (Fig. 4a). When a

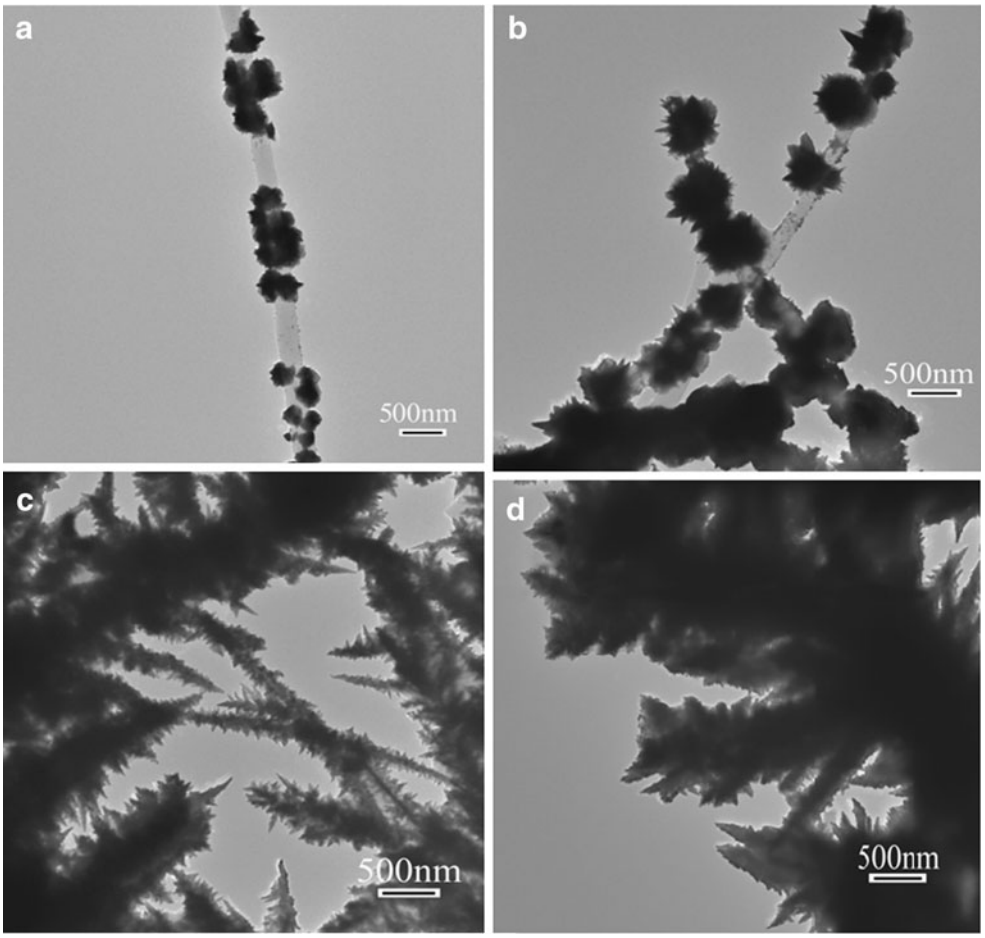

Fig. 3 TEM images of Pd/CNFs with different deposition times (**a** 1.0, **b** 2.0, **c** 4.0, and **d** 8.0 h). Deposition potential, −0.2 V

subcritical point is reached, Pd nanonuclei grow to supercritical clusters, as shown in Fig. 4b. With continuous increase in deposition time, Pd clusters with sufficient sizes grow along the κ direction, which leads to the formation of nanotree-like Pd clusters, as shown in Fig. 4c. This is because sulfuric acid anions such as HSO_4^- or SO_4^{2-} in the deposition solution are readily adsorbed on the Pd (111) surface, disturbing their growth to the plane [28,29]. The sulfuric acid anions are known to adsorb on the (111) surface of metal electrodes especially with an face-centered cubic (fcc) crystal structure, which have also been observed in the adsorption of bisulfate and sulfate on a Pt (111) electrode by Kolics and Wieckowski [30]. The adsorption of sulfuric acid anions on Pd (111) is more favorable than that on other planes, and hence, the Pd growth is always along the κ direction [31].

However, it is much harder for the edge site of the Pd clusters to adsorb sulfuric acid anions, which, along with higher Pd deposition amount, result in the merging of some branches in nanotree-like clusters.

XRD analysis and BET values of nano-engineered Pd/CNFs

XRD patterns obtained from electrospun CNFs and nano-engineered Pd/CNFs are presented in Fig. 5. The diffraction peak at 25.5° can be assigned to the diffraction of the (002) plane of graphite layers. The XRD pattern of Pd/CNFs presents typical Pd diffraction peaks at 40.0° (111), 46.7° (200), 68.2° (220), 82.2° (311), and 86.7° (222), respectively, which confirm that Pd crystals are formed on the deposited nanofibers [27].

The surface area and pore size distribution of nano-engineered Pd/CNFs were obtained using the BET nitrogen adsorption method, and the results are shown in Fig. 6. It is seen that the average pore size of Pd/CNFs is around 15 nm, and the BET surface area is 114.4 m g^{-1}; in comparison, the surface area of pure electrospun CNFs is only 25.9 m^2 g^{-1} before the deposition of nano-engineered Pd. The increase in surface area can be ascribed to the formation of complex hierarchical Pd nanostructure on the surface of CNFs. These results are complementing the findings obtained from TEM and SEM analyses.

Influence of deposition potential

As mentioned above, at a deposition potential of −0.2 V for 4.0 h, Pd nanocactus structure is formed on CNFs (Figs. 1 and 2). The effect of deposition potential on the Pd deposition structure can be seen in the SEM images shown

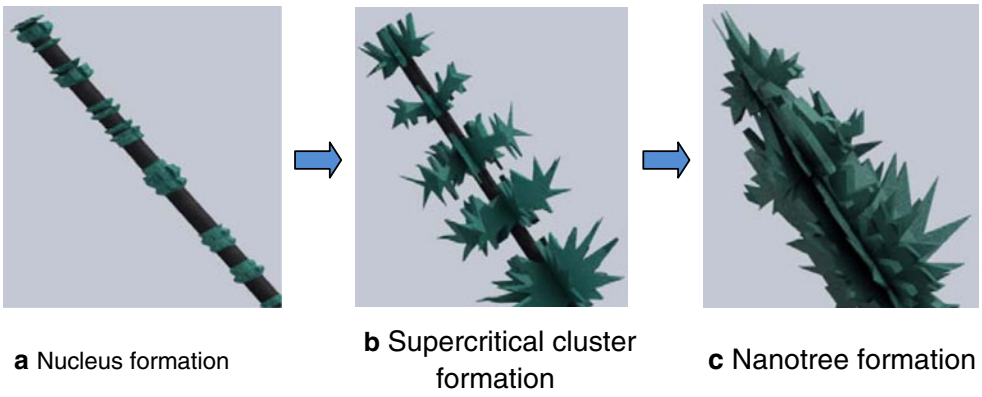

Fig. 4 Schematic representation of the growth mechanism of nanotree-structured Pd on a CNF. Deposition potential, −0.2 V. **a** Nucleus formation. **b** Supercritical cluster formation. **c** Nanotree formation

in Fig. 7. An increase in potential from −0.2 to −0.1 V causes the transformation of nanocactus structure to a nanoflower one. Further increase in the deposition potential in the noble direction (more positive) causes the nanoflower structure to disappear gradually, leaving only spherical Pd nanoparticles on the surface of CNFs.

During the formation of Pd critical nucleus, crystallizational overvoltage is the major parameter in determining the rate of nucleation in electrochemical crystallization. The relationship between the nucleation and growth rates of crystals can be discussed in terms of Pd grain size. Typically, at high rates of nucleation and slow growth of nanocrystals, fine-grained Pd deposits can be formed [32]. Assuming that each Pd nucleus gives one grain, the volume of grown Pd (V) is

$$V = iV_{\mathrm{pd}}/(JnF) \tag{1}$$

where i is the current density (milliamperes per square centimeter). V_{Pd} is the molar volume of Pd (cubic centimeters per mole), J is the nucleation rate (square centimeters per second), n is the amount of Pd (moles), and F is the faraday constant (coulombs per mole). Both i and J depend upon the overpotential η (V) of the process; thus, the corrected value of η is connected with i and J such that

$$\ln i = \ln i_{\mathrm{o}} + \alpha nF\eta/RT \tag{2}$$

and

$$\ln J = K_1 - K_2/\eta^2 \tag{3}$$

where α is the transfer coefficient (meters per second) and K_1 and K_2 are constants. Substitution of these expressions into Eq. 1 leads to

$$\ln V = \ln\left(V_{\mathrm{pd}}/nF\right) + \ln i_{\mathrm{o}} - K_1 + \alpha nF\eta/RT + K_2/\eta^2 \tag{4}$$

Differentiation of Eq. 4 is

$$\mathrm{d}\ln V/\mathrm{d}\eta = \alpha nF/RT - 2K_2/\eta^3 \tag{5}$$

The standard electrode potential for Pd^{2+}/Pd is 0.6927 V vs. Ag/AgCl/4.0 M KCl in aqueous solutions at 25 °C [33].

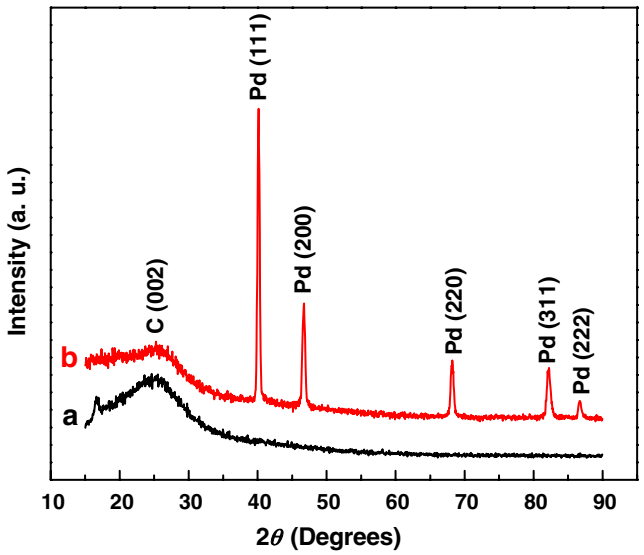

Fig. 5 XRD patterns of CNFs (*a*) and Pd/CNFs (*b*). Deposition potential, −0.2 V. Deposition time, 4.0 h

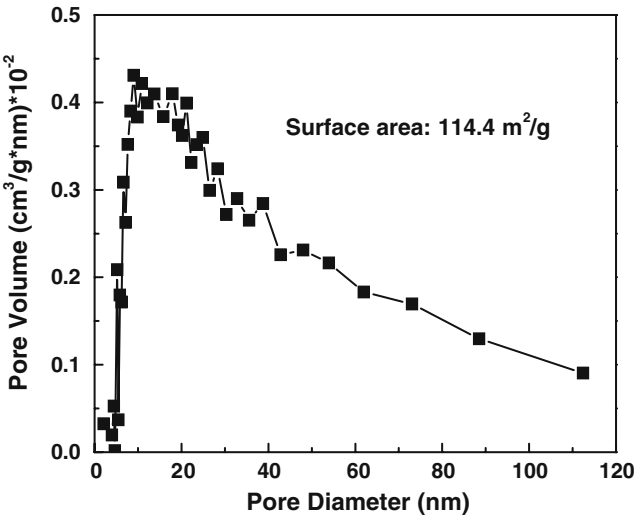

Fig. 6 Pore-size distribution of Pd/CNFs. Deposition potential, −0.2 V. Deposition time, 4.0 h

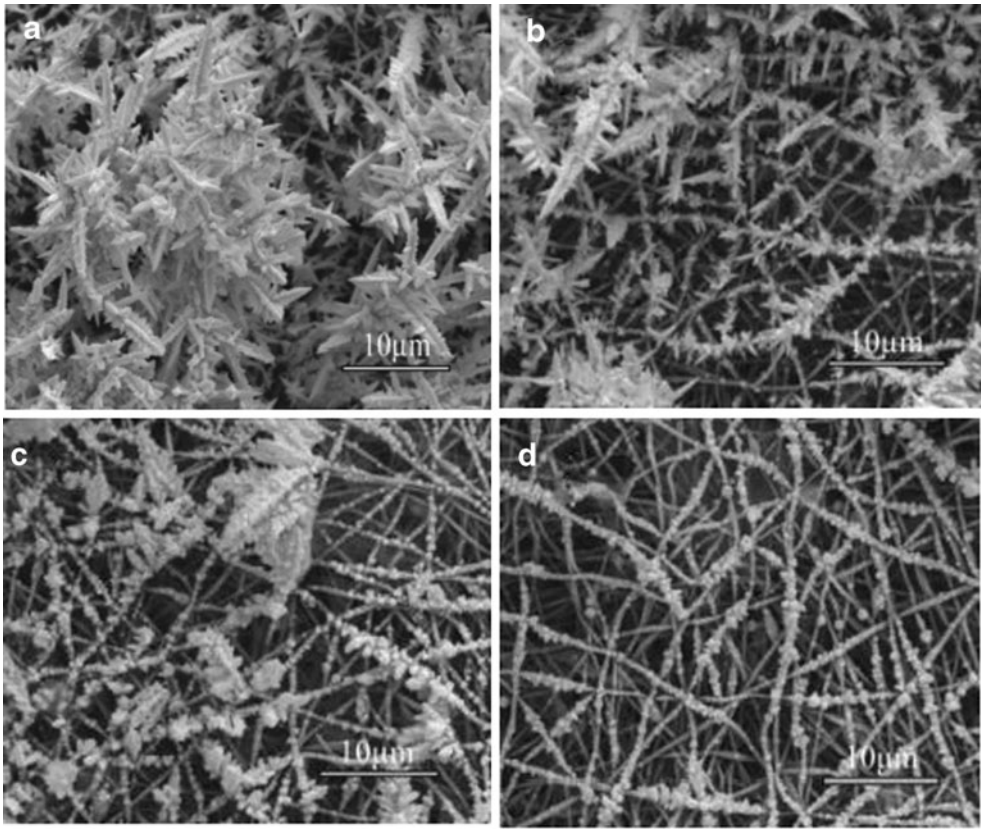

Fig. 7 SEM images of Pd/CNFs prepared with different electrodeposition potentials: **a** −0.1, **b** 0.0, **c** +0.1, and **d** +0.2 V. Deposition time, 4.0 h

According to Eq. 5, with increase in deposition overpotential η in the noble direction, the grain size increases [34]. In this work, all electrodeposition experiments were conducted underpotentials, i.e., negative overpotentials. Therefore, the increase of the negative overpotential in the noble direction results in the decrease of the grain size, which should be responsible for the gradual disappearance of Pd nanocactus structure on the CNF surface at higher deposition under potentials (Fig. 7c, d). In addition, based on XRD analyses (not shown in the Figure), Pd were deposited on the surface of CNFs under the four potentials (i.e., −0.1, 0.0, +0.1, and +0.2 V), which confirms that Pd

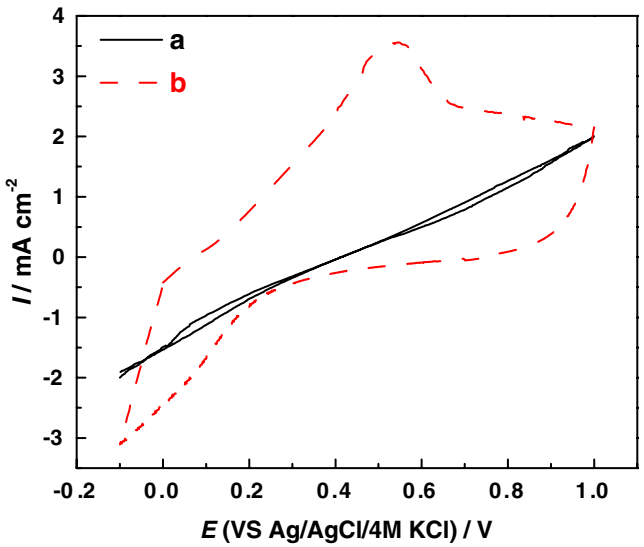

Fig. 8 Current density–potential curves of *a* CNF and *b* Pd/CNF electrodes in N_2-saturated 5 mM H_2O_2 + PBS solution. Deposition potential, −0.2 V. Deposition time, 4.0 h. Scan rate, 50.0 mV s^{-1}

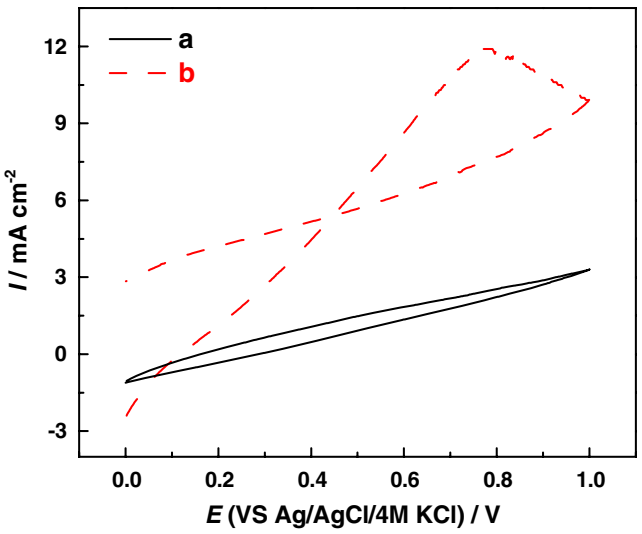

Fig. 9 Current density–potential curves of *a* CNF and *b* Pd/CNF electrodes in N_2-saturated 2 mM β-NADH + PBS solution. Deposition potential, −0.2 V. Deposition time, 4.0 h. Scan rate, 50.0 mV s^{-1}

Table 1 Electrochemical characteristics of Pd/CNF composites with different deposition durations toward the electrocatalytic redox of H_2O_2 (solution: N_2-saturated 5 mM H_2O_2 + PBS) and oxidation of β-NADH (solution: N_2-saturated 2 mM β-NADH + PBS)

Deposition duration (h)	Morphology	H_2O_2 redox peak current density (mA cm^{-2})	β-NADH oxidation peak current density
1.0	Snow-like particles	0.77	2.03
2.0	Snow-like particles	1.87	5.56
4.0	Tree-like clusters	3.56	11.90
8.0	Merged tree-like clusters	3.23	10.37

Deposition potential, −0.2 V. Scan rate, 50.0 mV s^{-1}

deposition also diminishes gradually when the potential increases in the noble direction.

Electrocatalytic redox of H_2O_2 and oxidation of β-NADH

The detection and quantitative determination of H_2O_2 has become extremely important in recent years because of its widely spread uses in food, pharmaceutical, chemical, and biochemical industries. Oxidation or reduction over electrode materials can be used in the direct electrochemical detection of H_2O_2 [35–38]. In order to evaluate the catalytic activity of nano-engineered Pd/CNF electrodes for the redox reaction of H_2O_2, cyclic voltammetry was conducted on CNF and Pd/CNF electrodes. Figure 8 shows current density–potential curves of CNF and Pd/CNF electrodes in N_2-saturated 5 mM H_2O_2 in PBS solution in water (pH= 7.2) at a scan rate of 50.0 mV s^{-1}. From Fig. 8, it is seen that there is almost no redox peak for the CNF electrode; however, both oxidation and reduction peaks of H_2O_2 can be found on the Pd/CNF electrode. The electro-oxidation of H_2O_2 starts at +0.40 V and forms a maximum peak at +0.52 V; however, such electro-oxidation peak was not found in the electrocatalytic activities of spherical Pd nanoparticle-loaded CNFs [27]. Moreover, the reduction of H_2O_2 below +0.20 V is also found when scanning back, which is comparable to that of spherical Pd nanoparticle-loaded CNFs [27]. The results demonstrate that nano-engineered Pd formed on the CNF surface has high catalytic activity for the redox reactions of H_2O_2, which make them suitable for use as the biosensor for H_2O_2 detection and can be operated at low working potentials.

In addition to the electrocatalytic redox of H_2O_2, Pd/CNFs display high electrocatalytic activity toward the oxidation of β-NADH, an important coenzyme in a number of dehydrogenase enzymatic reactions [37,39]. Figure 9 displays the oxidation curves of β-NADH using CNFs and Pd/CNFs in N_2-saturated 2 mM β-NADH + PBS solution. There is no peak found in the curve of CNFs; however, the Pd/CNF electrode yields a current density peak at +0.78 V. Such a large change in the oxidation of β-NADH indicates the high electrocatalytic activity of Pd/CNFs. The background current of the Pd/CNF electrode is much larger than that of bare CNF electrode and that of spherical Pd nanoparticle-loaded CNFs [27], attributing to the large electroactive surface area of Pd/CNFs. These results suggest that Pd/CNFs could be used to directly detect β-NADH at relatively low potentials without the need of redox mediators to shuttle the electrons from β-NADH.

Moreover, in order to study the electrochemical performance toward the redox of H_2O_2 and oxidation of β-NADH, the electrochemical characteristics of Pd/CNF composites with different deposition durations and different morphologies are summarized in Table 1. It is seen that with increase in Pd metal loading, the peak current densities of both H_2O_2 redox and β-NADH oxidation increase first and then reach a maximum when the deposition time is 4.0 h, which should be due to the formation of nano-engineered tree-like Pd depositions, which have large surface area, as demonstrated in Fig. 6.

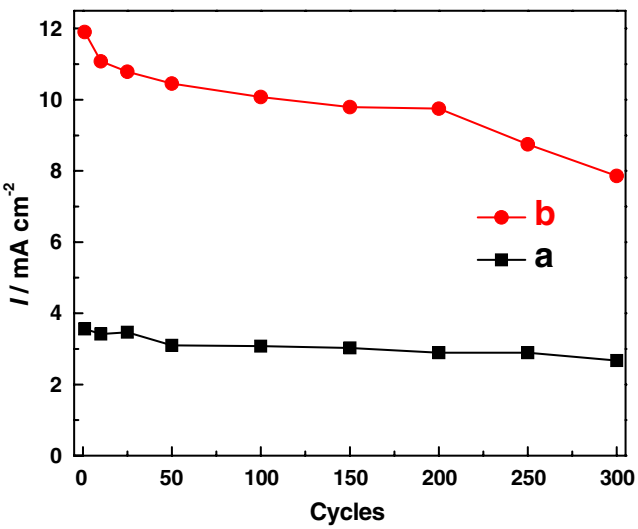

Fig. 10 Stability of Pd/CNFs toward the electrocatalytic redox of H_2O_2 (*a* solution: N_2-saturated 5 mM H_2O_2 + PBS) and oxidation of β-NADH (*b* solution: N_2-saturated 2 mM β-NADH + PBS). Deposition potential, −0.2 V. Deposition time, 4.0 h. Scan rate, 50.0 mV s^{-1}

Stability of Pd/CNFs

In order to study the long-term stability of Pd/CNFs, the peak current density (I_f) was measured as a function of cycle number toward the electrocatalytic redox of H_2O_2 and oxidation of β-NADH, respectively, and the results are shown in Fig. 10 c. I_f of Pd/CNFs toward the electrocatalytic redox of H_2O_2 is about 2.67 mA g^{-1}, which is 75% of the initial I_f. In comparison, after 300 cycles, the I_f of Pd/CNFs toward the oxidation of β-NADH is around 7.96 mA g^{-1}, which is 67% of the initial I_f. In general, the gradual decrease of the catalytic activity after successive cycling should be due to the slow degradation of engineered Pd nanoparticles on the surface of CNFs. Moreover, when compared to the I_f of Pd/CNFs toward the oxidation of H_2O_2, the I_f of Pd/CNFs toward the electrocatalytic redox of β-NADH is much higher (i.e., 11.90 vs. 3.56 mA cm^{-2} at the first cycle), which may indicate that the selectivity of Pd/CNFs in the oxidation of β-NADH is much better than that of the redox of H_2O_2.

Conclusions

Pd/CNFs with well-defined morphology were prepared by electrodepositing nano-engineered Pd onto electrospun carbon nanofibers under different deposition durations and potentials. TEM and SEM results show that both deposition duration and potential have important influence on the morphology of nano-engineered Pd on the surface of CNFs. With the increase of deposition time from 1.0 to 4.0 h, nanocactus Pd composed of nanotree-like clusters were gradually formed on the surface of CNFs under the potential −0.2 V, and they have a relatively high surface area. As the deposition potential increases, the nanocactus structure disappears because of diminishing grains. The resulting Pd/CNF electrodes were found to display high electrocatalytic activities toward the redox of H_2O_2 and oxidation of β-NADH, which are difficult to be obtained in spherical Pd nanoparticle-loaded CNFs and make them promising candidates for applications in food, pharmaceutical, chemical, and biochemical industries.

Acknowledgment This work was supported by the US National Science Foundation (0833837), National Textile Center (ITA-08-07400), and ACS Petroleum Research Fund (47863-G10).

References

1. Miyaura N, Suzuki A (1995) Chem Rev 95:2457–2483
2. Narayanan R, El-Sayed MA (2004) Nano Lett 4:1343–1348
3. Stille JK (1986) Angew Chem Int Ed 25:508–523
4. Tatamidani H, Kakiuchi F, Chatani N (2004) Org Lett 6:3597–3599
5. Tian N, Zhou ZY, Sun SG, Ding Y, Wang ZL (2007) Science 316:732–735
6. Meng H, Sun S, Masse JP, Dodelet JP (2008) Chem Mater 20:6998–7002
7. Choo H, He BL, Liew KY, Liu HF, Li JL (2006) J Mol Catal A Chem 244:217–228
8. Teng XW, Han WQ, Ku W, Hucker M (2008) Angew Chem Int Ed 47:2055–2058
9. Xiong YJ, Cai HG, Wiley BJ, Wang JG, Kim MJ, Xia YN (2007) J Am Chem Soc 129:3665–3675
10. Xiong YJ, McLellan JM, Chen JY, Yin YD, Li ZY, Xia YN (2005) J Am Chem Soc 127:17118–17127
11. Hu FP, Wang Z, Li Y, Li C, Zhang X, Shen PK (2008) J Power Sources 177:61–66
12. Sun YP, Fu KF, Lin Y, Huang WJ (2002) Acc Chem Res 35:1096–1104
13. Saini RK, Chiang IW, Peng H, Smalley RE, Billups WE, Hauge RH, Margrave JL (2003) J Am Chem Soc 125:3617–3621
14. Chen JH, Li WZ, Wang DZ, Yang SX, Wen JG, Ren ZF (2002) Carbon 40:1193–1197
15. Tsai MC, Yeh TK, Tsai CH (2006) Electrochem Commun 8:1445–1452
16. Bower C, Zhu W, Shalom D, Lopez D, Chen LH, Gammel PL, Jin S (2002) Appl Phys Lett 80:3820–3822
17. Wang SG, Zhang Q, Wang RL, Yoon SF (2003) Biochem Biophys Res Commun 311:572–576
18. Xing YC (2004) J Phys Chem B 108:19255–19259
19. De Jong KP, Geus JW (2000) Cat Rev-Sci Eng 42:481–510
20. Gibson P, Schreuder-Gibson H, Rivin D (2001) Colloids Surf A 187–188:469–481
21. Guillorn MA, McKnight TE, Melechko A, Merkulov VI, Britt PF, Austin DW, Lowndes DH, Simpson ML (2002) J Appl Phys 91:3824–3828
22. Smita E, Bűttnerb U, Sanderson RD (2005) Polymer 46:2419–2423
23. Tribolet P, Kiwi-Minsker L (2005) Catal Today 105:337–343
24. Winter F, Bezemer GL, Spek C, Meeldijk JD, Dillen AJ, Geus JW, Jong KP (2005) Carbon 43:327–332
25. Yang WQ, Yang SH, Guo JS, Sun GQ, Xin Q (2007) Carbon 45:397–401
26. Zhao TJ, De C, Dai YC, Yuan WK, Holmen A (2007) Top Catal 45:87–91
27. Huang JS, Wang DW, Hou HQ, You TY (2008) Adv Funct Mater 18:441–448
28. Hoshi N, Kuroda M, Koga O, Hori Y (2002) J Phys Chem B 106:9107–9113
29. Nakamura M, Sakurai Y, Ito M (2004) J Electroanal Chem 563:63–69
30. Kolics A, Wieckowski A (2001) J Phys Chem B 105:2588–2595
31. Song YJ, Kim JY, Park KW (2009) Cryst Growth Des 9:505–507
32. Natter H, Hempelmann R (1996) J Phys Chem B 100:19525–19532
33. Bard AJ, Parsons R, Jordan J (1985) Standard potentials in aqueous solution. Marcel Dekker, New York
34. Gamburg YD (2005) Metal electrodeposition, chapter 2, pp 47–77
35. Cai XH, Kalcher K, Kolbl G, Neuhold C, Diewald W, Ogorevc B (1995) Electroanalysis 7:340–345
36. Domenech A, Alarcon J (2002) Anal Chim Acta 452:11–22
37. Wang J (2002) Talanta 56:223–231
38. Welch CM, Banks CE, Simm AO, Compton RG (2005) Anal Bioanal Chem 382:12–21
39. Pandey PC, Upadhyay S, Upadhyay AK (2004) Sens Actuators B 102:126–131